HHS Public Access

Author manuscript

J Biomed Mater Res A. Author manuscript; available in PMC 2019 June 05.

Published in final edited form as:

J Biomed Mater Res A. 2019 April ; 107(4): 884–892. doi:10.1002/jbm.a.36605.

Polymer scaffold architecture is a key determinant in mast cell inflammatory and angiogenic responses

Daniel Abebayehu[1], **Andrew J. Spence**[2], **Michael J. McClure**[1], **Tamara T. Haque**[2], **Kevin O. Rivera**[2], and **John J. Ryan**[2]

[1]Department of Biomedical Engineering, Virginia Commonwealth University, Richmond, Virginia 23284

[2]Department of Biology, Virginia Commonwealth University, Richmond, Virginia 23284-2012

Abstract

Implanted polymer scaffolds can induce inflammation leading to the foreign body response (FBR), fibrosis, and implant failure. Thus, it is important to understand how immune cells interact with scaffolds to mitigate inflammation and promote a regenerative response. We previously demonstrated that macrophage phenotype is modulated by fiber and pore diameters of an electrospun scaffold. However, it is unclear if this effect is consistent among other innate immune cells. Mast cells are inflammatory sentinels that play a vital role in the FBR of implanted biomaterials, as well as angiogenesis. We determined if altering electrospun scaffold architecture modulates mast cell responses, with the goal of promoting regenerative cell-scaffold interactions. Polydioxanone (PDO) scaffolds were made from 60 mg/mL or 140 mg/mL PDO solutions, yielding structures with divergent fiber and pore diameters. Mouse mast cells plated on these scaffolds were activated with IL-33 or lipo-polysaccharide (LPS). Relative to the 60 mg/mL scaffold, 140 mg/mL scaffolds yielded less IL-6 and TNF, and greater VEGF secretion. Pores >4–6 μm elicited less IL-6 and TNF secretion. IL-33-induced VEGF regulation was more complex, showing effects of both pore size and fiber diameter. These data indicate parameters that can predict mast cell responses to scaffolds, informing biomaterial design to increase wound healing and diminish implant rejection.

Keywords

polydioxanone; inflammation; mast cell; angiogenesis

INTRODUCTION

For any implanted biomaterial, an important factor to consider is the immune response and how to mitigate inflammation. Surgical pathologists have noted the persistence of the foreign body response (FBR) of retrieved implants, which is due to chronic/unresolved inflammation.[1] Inflammation is not meant to be avoided altogether, but rather spatially and

Correspondence to: John Ryan; jjryan@vcu.edu.

CONFLICTS OF INTEREST

The authors have no conflicts of interest related to this work.

temporally controlled because inflammation has been shown to be critical for beneficial outcomes, such as angiogenesis.[2] If the response to an implant elicits a milieu of pro-healing factors, the implant is more likely to succeed. Yet, implantation can prompt unresolved inflammation, frustrated phagocytosis, and macrophage fusion to form foreign body giant cells.[3] This is true with polymeric materials due to how immune cells can recognize polymers with their pattern recognition receptors (PRR; e.g., toll-like receptors or scavenger receptors).[4,5] This sustained PRR signaling can lead to fibrotic encapsulation of the biomaterial, contributing to implant failure, and persistent pain.[6–10] Biomaterial design can alter this outcome, but the mechanisms by which polymer architecture alters immunity has yet to be fully determined. Innate immune cells are understood to determine the fate of implanted biomaterials.[11] While there has been considerable attention given to macrophages and neutrophils, much less is known about mast cell–biomaterial interactions.

Mast cells are innate sentinels located in all tissues except blood. They are abundant in connective and mucosal tissues where interactions with the external environment are common, including the skin, gut, and lungs.[9] Mast cells play an essential role in wound healing, inflammation, angiogenesis, tissue remodeling, and the FBR.[12–18] Similar to macrophages, mast cells originate in the bone marrow from the common myeloid progenitor, migrate to the vasculature as a mast cell progenitor, and fully mature in tissues, where their functional phenotype is plastic and determined by the micro-environment. Mature mast cells are often situated perivascularly and can have profound effects on vascular tone, edema, and angiogenesis.[19,20] When angiogenesis occurs during remodeling, it is preceded or accompanied by macrophage and neutrophil influx that has been argued to be mast cell-mediated.[15] Once activated, mast cells produce myriad factors, including transforming growth factor (TGF-β1), fibroblast growth factors (FGF-1 and FGF-2), interleukin-8 (IL-8), vascular endothelial growth factor (VEGF), and many proteases that alter tissue structure and growth factor availability.[21,22] Therefore, biomaterial implants designed to shape mast cell function to suppress inflammation and promote wound healing will have a greater capacity for regeneration, yielding improved therapeutic outcomes.

One hypothesized way of controlling innate immune responses to electrospun scaffolds is to alter implant architecture, such as porosity and fiber diameter. There has been considerable work exploring how scaffold pore size affects implant function and success.[3,23] Altering pore size in engineered structures can influence both angiogenesis and macrophage polarization.[24,25] Additionally, scaffold fiber diameter affects inflammatory cytokine production.[26] Our group previously found that increasing scaffold pore size and fiber diameter promotes macrophage M2 polarization.[27] However, very little work has assessed how mast cells respond to scaffolds, despite the important role they play in inflammation, wound healing, and angiogenesis.[4,28,29] In this study, we examine the importance of pore and fiber size on mast cell activation by the common innate immune signals, LPS and IL-33. We find evidence that increasing both pore diameter and fiber size reduces inflammatory responses and increases pro-angiogenic effects. These data help instruct rational design of biomaterials to promote implant success.

MATERIALS AND METHODS

Electrospinning

Electrospinning was used to create fibrous scaffolds of various morphologies made from polydioxanone (PDO) (Ethicon Inc.). PDO was dissolved in 1,1,1,3,3,3, Hexafluoro-2-isopropanol (HFP) at either 60 or 140 mg/mL in a scintillation vial. The polymer solutions were then aspirated into 5 mL syringes with 18-gauge blunt tip needles. The syringe was then loaded into a KDS 100 Legacy Syringe Pump (KD Scientific, Holliston, MA) and the polymer solution was dispensed at a 6 mL/h rate. Polymer solutions were electrospun across a gap distance of 12 cm onto a rotating rectangular stainless steel mandrel (0.5 cm × 3 cm 1.5 cm) or onto a perforated air-flow mandrel with an inlet pressure of 50 kPa.[30] All scaffolds were electrospun with an applied voltage of 25 kV and a mandrel rotating at a speed of 400 rpm. To reduce pore size in electrospun scaffolds, scaffolds underwent uniform compression by placing the scaffolds between two flat stainless blocks and using a hydraulic press at 5000 psi (Carver Inc., Wabash, IN). After electrospinning, scaffold samples were imaged using either a Zeiss Auriga FIB-SEM scanning electron microscope (SEM) (Zeiss, Oberkochen, Germany). Scanning electron micrographs were analyzed to measure fiber and pore diameter using ImageJ. Fiber diameter measurements were collected by measuring the diameter of at least 60 individual fibers from different segments of the micrographs in order to avoid replicate measurements. Pores to be measured in ImageJ were designated as pores based on being interstitial spaces between fibers on what appear to be on the same plane, and pore diameter was defined by recording the average between length and width.

X-ray photoelectron spectroscopy

Relative atomic concentration and chemical bonding information were obtained from the specimen surfaces by x-ray photoelectron spectroscopy (Thermo K-Alpha XPS; Thermo Fisher Scientific, West Palm Beach, FL). The XPS instrument was equipped with a monochromatic Al Kα X-ray source ($h\nu$ = 1486.6 eV). Spectra were collected at 5×10^{-8} mbar or lower using an X-ray spot size of 400 μm and a pass energy of 100 eV, with 1 eV increments, at a 55° takeoff angle. Three specimens of PDO 60 and 140 mg/mL fiber scaffolds were scanned three times each and all values were averaged.

Reagents

Recombinant mouse IL-3, IL-33, and stem cell factor (SCF), as well as ELISA kits to detect mouse IL-6, TNF, and MCP-1 (CCL-2) were purchased from BioLegend (San Diego, CA). Mouse MIP-1α (CCL-3) and VEGF ELISA kits were purchased from PeproTech (Rocky Hill, NJ). Lipopolysaccharide (LPS) from *Escherichia coli* 055:B5 was purchased from Sigma-Aldrich (catalog no. L4524, St. Louis, MO).

Cell culture and cell seeding

Following electrospinning, 10 mm disks were produced using biopsy punches and disinfected by soaking in 70% ethanol for 15 min and washed twice with 1X PBS. To promote mast cell adhesion, scaffold disks were incubated in fibronectin (R&D Systems, Minneapolis, MN) at 50 μg/mL for 1 h at 37°C. After incubation, scaffolds were moved to a

new well to avoid residual fibronectin, and a cloning ring (Thermo Fisher, Waltham, MA) was added to keep the scaffold from folding and to localize cells to the scaffold. Bone marrow-derived mast cells (BMMC) were developed by harvesting bone marrow from the tibias and femurs of euthanized C57BL/6 mice. Mice were used with approval of the Virginia Commonwealth University Institutional Animal Care and Use Committee. Bone marrow cells were cultured for 3 weeks in complete RPMI (cRPMI) 1640 medium (Invitrogen Life Technologies, Carlsbad, CA) containing 10% FBS, 2 m*M* L-glutamine, 100 U/mL penicillin, 100 μg/mL streptomycin, 1 mM sodium pyruvate, and 1 m*M* HEPES (all from Corning, Corning, NY), supplemented with IL-3-containing supernatant from WEHI-3B cells and SCF-containing supernatant from BHK-MKL cells. The final concentrations of IL-3 and SCF were adjusted to 1.5 ng/mL and 15 ng/mL, respectively, as measured by ELISA. BMMC were used after 3 weeks of culture, at which point these populations were >90% mast cells, based on staining for c-Kit and FceRI expression. BMMC were seeded at 1×10^6 cells/mL on fibronectin-coated scaffolds with a cloning ring, in cRPMI with IL-3 and SCF at 10 ng/mL each. Cells were plated directly onto the scaffolds and not disturbed before adding the activation stimuli. The wells were inspected by light microscopy to ensure survival and adhesion. After 48-h incubation on fibronectin-coated scaffolds, IL-33 (100 μg/mL) or LPS (1 μg/mL) was added to activate cells.

RT-qPCR

Bone marrow-derived mast cells were seeded on scaffolds and activated with 100 ng/mL of IL-33 for 6 h. Scaffolds were then placed in TRIzol reagent (Life Technologies, Grand Island, NY) to extract RNA, which was measured using a Thermo Scientific NanoDrop 1000 UV–vis Spectrophotometer (Thermo Fisher, Waltham, MA). cDNA was produced using a qScript cDNA Synthesis Kit from Quanta Biosciences (Gaithersburg, MD), and amplified using PerfeCTa SYBR Green SuperMix (Quanta Biosciences, Gaithersburg, MD) on the Bio Rad CFX96 Touch™ Real-Time PCR Detection System (Bio-Rad, Hercules, CA). Primers were purchased from Euro-fins MWG Operon (Huntsville, AL). The following primers were used:

IL-6 forward, 5′-TCCAGTTGCCTTCTTGGGAC-3′; IL-6 reverse, 5′-TCCAGTTGCCTTCTTGGGAC-3′; TNF forward, 5′-AGCACAGAAAGCATCATCCGC-3′; TNF reverse, 5′-TGCCACAAG CAGGAATGAGAAG- 3′; VEGF forward, 5′-GAGGATGTCCTCAC TCGGATG-3′; VEGF reverse, 5′-GTCGTGTTTCTGGAAGTGAGC AA-3′; MMP-9 forward, 5′-GCCCTGGAACTCACACGACA-3′; MMP-9 reverse, 5′-TTGGAAACTCACACGCCAGAAG-3′; TGFβ−1 forward, 5′-GTGTGGAGCAACATGTGGAACTCTA-3′; TGFβ−1 reverse, 5′-TTGGTTCAGCCACTGCCGTA-3′; FGF-2 forward, 5′-CC AACCGGTACCTTGCTATG-3′; FGF-2 reverse, 5′-TATGGCCTTC TGTCCAGGTC-3′; β-actin forward, 5′-GATGACGATATCGCTGCGC −3′; β-actin reverse, 5′-CTCGTCACCCACATAGGAGTC-3′.

Statistical analysis

Data are presented as mean ± SE and analyzed using Graph-Pad Prism 6 software (GraphPad, La Jolla, CA). Comparisons between two groups were done using unpaired Student's *t*-test; comparisons between multiple groups were done using one-way analysis of variance with Tukey's post-hoc test. All $p < 0.05$ were deemed significant.

RESULTS

Fabrication of electrospun scaffolds

We electrospun scaffolds with the lowest and highest PDO concentrations possible, 60 mg/mL and 140 mg/mL, in order to produce scaffolds with the most divergent architectures. PDO concentrations below 60 mg/mL led to uneven dispersal at the needle tip and failed to produce a usable scaffold, while concentrations above 140 mg/mL were too viscous to consistently generate scaffolds. Figure 1 shows electron micrographs of PDO scaffolds from these solutions. 60 mg/mL scaffolds featured fibers with a diameter of 400 nm and pores with an approximate diameter of 1.5 μm, while 140 mg/mL scaffolds contained fibers with a diameter of 2.4 μm and pores with a diameter of 18 μm. These large differences are consistent with our previous observations,[27] and permitted us to examine how scaffold architecture alters mast cell inflammatory responses.

Surface chemistry of electrospun scaffolds

X-ray photoelectron spectroscopy was performed on 60 and 140 mg/mL PDO scaffolds to determine if any concentration-dependent differences in surface chemistry occurred. Overall, we demonstrated that surface chemistry was unchanged between electrospun PDO fibers at 60 and 140 mg/mL. Specifically, carbon and oxygen ratios were unaffected by solvent, electrospinning, and concentration when comparing 60, 140, and pure PDO pellet (Fig. 2A). In addition, carbon and oxygen binding energy peaks for electropun PDO fibers were identical (Fig. 2B,C). Interestingly, carbon binding energy for pure PDO polymer was different from electrospun fibers, while oxygen was unaffected by electrospinning, These similarities in surface chemistry supported our hypothesis that the mast cell response to electrospun scaffolds was dependent on fiber architecture.

Altered mast cell cytokine production on scaffolds of varying architecture

Mast cells adhere poorly to uncoated PDO, but we previously found that they adhere to fibronectin-coated PDO scaffolds.[29] Because fibronectin is present at the wound site, abundant at fibrotic encapsulations, and present at high concentrations in plasma,[31,32] we used fibronectin-coated scaffolds in our studies. Importantly, these scaffolds alone elicit little mast cell activation.[29] In the context of tissue damage and/or infection, IL-33 and LPS should be abundant. IL-33 is produced by tissue resident endothelial, epithelial and fibroblast cells upon damage, while LPS is often present at wound site due to bacterial contamination.[33–35] Therefore, we examined how fibronectin-coated scaffolds with varying morphologies altered IL-33- and LPS-mediated mast cell cytokine production.

Bone marrow-derived mast cells were seeded on PDO scaffolds and 48 h later were activated +/− LPS or IL-33. Supernatants were collected after 16 h and analyzed via ELISA. Figure

3A shows that scaffold type greatly altered the mast cell response to IL-33 or LPS. Mast cells on 60 mg/mL polymers produced significantly more IL-6 than cells cultured on 140 mg/mL membranes. In fact, the 140 mg/mL scaffold cultures produced less IL-6 than the tissue culture plastic (TCP) control. TNF secretion was similarly affected by scaffold architecture, but only in response to IL-33 activation. Interestingly, there was selectivity to these effects, since MCP-1 and MIP-1α chemokine production was unchanged by scaffold structure (Fig. 3B). These data demonstrate that scaffold architecture can shape mast cell responses to innate immune signals, and are analogous to our earlier finding that macrophage phenotype is altered by differing PDO scaffolds.[27]

While we found differences in cytokine protein secreted in the culture supernatants, fibronectin, which contains a growth factor-binding domain,[36] is present on the scaffolds. It is possible that the changes in cytokine detection could be attributed to IL-6 or TNF sequestration at the scaffold surface via fibronectin binding. Therefore, cytokine mRNA induction was measured to confirm our protein findings. BMMC seeded on fibronectin-coated 60 and 140 mg/mL PDO scaffolds were activated +/− IL-33. As observed at the protein level, 60 mg/mL PDO scaffolds elicited greater IL- 33-mediated IL-6 and TNF expression than 140 mg/mL structures (Fig. 3C).

Scaffold pore size is critical to regulating the mast cell inflammatory response

The 60 mg/mL and 140 mg/mL scaffolds differ in two key features: fiber diameter and pore size. To isolate the contributions of these variables, we sought ways of altering pore size without changing fiber diameter in the two scaffold types. First, we created 60 mg/mL scaffolds using an air-flow (AF) mandrel approach,[30] which increases porosity throughout the scaffold. This technique tripled average pore size from approximately 1.5 μm to 4.5 μm while maintaining the fiber diameter at 400 nm (Fig. 4A,B). BMMC were seeded on 60 mg/mL scaffolds generated with solid or AF mandrels, and activated +/− IL-33 or LPS. 16 h later, supernatants were collected and analyzed via ELISA. Culture on AF mandrel-produced scaffolds significantly reduced IL-6 and TNF secretion in response to IL-33 or LPS, compared to scaffolds generated on a solid mandrel (Fig. 4C). This demonstrates that between scaffolds with the same fiber diameter, increasing pore size can reduce inflammatory cytokine secretion.

To complement the AF mandrel studies, we reduced pore size on the 140 mg/mL scaffolds. Scaffolds were compressed using a hydraulic press that provided uniform pressure across the structure. As shown in Figure 5A and B, compression reduced pore size from approximately 18 μm to 6 μm on the 140 mg/mL scaffolds without altering fiber diameter. BMMC seeded onto 140 or 140 compressed (C) scaffolds were activated +/− IL-33 or LPS, and supernatants were analyzed via ELISA. Surprisingly, LPS-induced IL-6 and TNF secretion was unchanged by compressing the 140 mg/mL scaffolds. Further-more, IL-33-induced cytokine changes were inconsistent (Fig. 5C). IL-33-mediated IL-6 production was moderately enhanced by compressing the scaffold, but TNF secretion was suppressed. These data suggest that with a fiber diameter of 2 μm, pore size changes have inconsistent effects on mast cell inflammatory responses. Additionally, it is possible that while we reduced the pore diameter to one third the original size, these dimensions may still be above a threshold

required to promote inflammatory cytokines. For example, the 60 mg/mL scaffold has pores of 2 μm diameter (Fig. 1).

VEGF regulation shows effects of both pore size and fiber diameter

Because angiogenesis is a critical aspect of wound healing at the biomaterial implant site, we also examined VEGF production using these scaffolds. LPS induced little VEGF (not shown), but we noted significant production from IL-33-stimulated cells. As shown in Figure 6, cells cultured on 60 mg/mL scaffolds produced little VEGF in response to IL-33, with no statistical significance. By comparison, 140 mg/mL scaffolds induced twice as much VEGF as the 60 mg/mL scaffold. Compressing the 140 mg/mL scaffold reduced IL-33-mediated VEGF secretion to a level comparable to the 60 mg/mL scaffold. This was consistent with the theory that smaller pores support an inflammatory rather than a wound healing response. However, expanding pore size on the 60 mg/mL scaffold by using an airflow mandrel did not rescue VEGF production. This may be due to inhibitory effects of the small fiber size. However, the 60AF structure still has relatively small pores (4.5 μm) compared to the 140 mg/mL scaffold (18 μm). Hence, we can conclude that VEGF production is supported best by scaffolds with large fibers and pores, which is greatly reduced by condensing either the fibers or pores.

DISCUSSION

Electrospinning offers great promise as a method for fabricating synthetic grafts that are inexpensive, potentially bioresorbable, and have off-the-shelf availability. Additionally, the sub-micron fiber diameters of electrospun scaffolds can mimic the structure and function of the native extracellular matrix (ECM).[37] However, a major limitation is the inability to finely control scaffold pore size, due to the tight packing of fibers.[30,38,39] Pore size is a critical structural component that has the capacity to alter wound healing, angiogenesis, and cellular infiltration into the scaffold.[40] Currently, clinically approved synthetic grafts undergo transanastomotic endothelialization (i.e., endothelium growth from the adjacent vessel into graft). However, this phenomenon provides very limited endothelium growth. This problem could be addressed by increasing pore size throughout an implant, facilitating transmural angiogenesis throughout the walls of the implant.[41] Likewise, fibroblast migration into the implant is important for tissue remodeling, and may also be facilitated by increasing the porosity of the implant.[42] Thus, it is imperative to find ways to alter scaffold architecture to improve functionality.

A critical variable dictating the fate of an implanted biomaterial is its initial interactions with the innate immune system. If the scaffold elicits an inflammatory response by cells such as macrophages, mast cells, dendritic cells, or neutrophils, the result can be fibrotic encapsulation and implant failure.[11,16] In this study, we sought to determine if changing electrospun scaffold architecture could alter the response of mast cells, a key sentinel cell of innate immunity. Our group has previously published that increasing pore size and fiber diameter promoted macrophage M2 polarization.[27] While the macrophage response to these scaffolds is important, macrophages do not respond to these materials independently or in

isolation. Therefore, it is important to examine other innate immune cells residing in peripheral tissue.

Scaffold pore size can be increased by creating larger fibers, achieved with greater polymer concentration during electrospinning. However, the pitfall with this method is losing the sub-micron fiber diameters mimicking native ECM. Previous work has shown that while scaffolds like those created with 60 mg/mL PDO have sub-micron fibers, their density promotes an inflammatory response.[43]Macrophages will fuse to form multinucleated foreign body giant cells (FBGCs) when met with a material they cannot infiltrate nor engulf, such as a dense scaffold with small pore size. In this scenario, FBGCs release highly inflammatory reactive oxygen species in an attempt to break down the material.[4,11,27] This relationship between implant architecture and inflammation prompted the goal to create scaffolds with sub-micron fiber diameters and increased pore size. This was accomplished using an air-flow mandrel. When testing mast cells, the 60AF scaffold promoted significantly less inflammatory cytokine production in response to IL-33 and LPS. In fact, the amount of IL-6 and TNF released was similar to the 140 mg/mL scaffold, which has fibers too large to mimic native ECM.

While the results of increasing pore size on the 60 mg/mL scaffold were clear, pore size effects were less obvious from studies of the 140 mg/mL structures. Compressing these scaffolds reduced pore diameter without affecting fiber size, but this had little or no effect on LPS- and IL-33-induced IL-6 and TNF secretion. A limitation of the compression approach was that pores could not be reduced below approximately 6 pm without damaging the scaffold. This pore size resembles the 60AF scaffold (4.5 μm) that reduced IL-33 and LPS responses to the 60 mg/mL scaffolds. These data suggest that mast cell inflammatory cytokine responses are elicited by a pore size threshold below the 4–6 μm range. Mast cells have an approximate diameter of 10–15 μm, and migrate through pores of at least 3 μm diameter.[44] Therefore, mast cells may engage the 140 and 140C scaffolds in a similar manner. In a previous study, we found that 140C scaffolds elicited a weaker M2 macrophage response than 140 mg/mL scaffolds.[27] That study did not assess inflammatory cytokine production, so direct comparisons are difficult. However, macrophages are considerably larger than mast cells and may therefore have a higher pore size “threshold” at which scaffolds elicit an inflammatory or M1 phenotype. We conclude that in the presence of large fibers, reducing pore size to 6 μm has little effect on inflammatory cytokine secretion from mast cells.

We assessed VEGF production as one measure of the angiogenic response. With larger fibers and pores, the 140 mg/mL scaffold elicited the strongest VEGF response, fitting our hypothesis that large pores are less inflammatory and can promote wound healing/angiogenesis. This theory was further supported by reduced VEGF secretion when compressing the 140 mg/mL scaffold pores. The 60 mg/mL scaffold, even when constructed on an airflow mandrel, did not elicit significant VEGF secretion. An important limit to our approach was the inability to create pores greater than about 4.5 μm with the airflow mandrel, which is still much smaller than the 18 μm pores of the 140 mg/mL scaffold. This limitation is important: because the 60 mg/mL fibers are closer to ECM dimensions,

reducing inflammation and increasing VEGF production on these scaffold would be optimal. At present, we can only achieve the former and not the latter.

A final point is that while macrophages do not require scaffold coating with an adhesion-promoting protein, mast cells do, as reported in our earlier study.[29] In this work, scaffolds were coated with fibronectin prior to mast cell seeding. Previous work has demonstrated the role of plasma fibronectin on scaffold fate and the FBR. When biomaterials were implanted in mice deficient in plasma fibronectin, fibrotic capsules were thicker and more foreign body giant cells were present. This indicates a critical role for plasma fibronectin in mitigating inflammatory responses to biomaterials.[28] This suggests that coating electrospun scaffolds with an appropriate adhesion protein may have physiological relevance.

CONCLUSIONS

In this study we demonstrate that LPS- and IL-33-mediated mast cell responses to electrospun scaffolds can be modulated by scaffold geometry, with a strong effect of pore size. Our findings suggest that a pore size at or above 4 μm diminishes inflammatory cytokine production, including on sub-micron fiber structures. The threshold at which other cell types are altered by pore size may differ and warrants further research. VEGF induction was more stringent, and may require both large fibers and pores. These results indicate important caveats for designing biomaterials that promote wound healing and minimize the inflammatory response that precipitates implant failure.

ACKNOWLEDGMENTS

This study was supported by NIH grants 1R01AI101153 and 2R01AI059638 to JJR.

Contract grant sponsor: National Institute of Allergy and Infectious Diseases; contract grant number: 1R01AI101153 and 2R01AI059638

REFERENCES

1. Anderson JM, Rodriguez A, Chang DT. Foreign body reaction to biomaterials. Semin Immunol 2008;20:86–100. [PubMed: 18162407]
2. Jones KS. Effects of biomaterial-induced inflammation on fibrosis and rejection. Semin Immunol 2008;20:130–136. [PubMed: 18191409]
3. Brown BN, Badylak SF. Expanded applications, shifting paradigms and an improved understanding of host-biomaterial interactions. Acta Biomater 2013;9:4948–4955. [PubMed: 23099303]
4. Avula MN, Rao AN, McGill LD, Grainger DW, Solzbacher F. Foreign body response to subcutaneous biomaterial implants in a mast cell-deficient Kitw-Sh murine model. Acta Biomater 2014;10:1856–1863. [PubMed: 24406200]
5. Love RJ, Jones KS. The recognition of biomaterials: Pattern recognition of medical polymers and their adsorbed biomolecules. J Biomed Mater Res 2013;101A:2740–2752.
6. Darby IA, Laverdet B, Bonté F, Desmouliere A. Fibroblasts and myo-fibroblasts in wound healing. Clin Cosmet Investig Dermatol 2014;7: 301–312.
7. Martinez FO, Sica A, Mantovani A, Locati M. Macrophage activation and polarization. Front Biosci 2008;13:453–461. [PubMed: 17981560]
8. Ribatti D, Crivellato E. Mast cells, angiogenesis, and tumour growth. Biochim Biophys Acta 2012;1822:2–8. [PubMed: 21130163]
9. Dwyer DF, Dwyer DF, Barrett NA, Austen KF, Kim EY, Brenner MB, Shaw L, Yu B, Goldrath A, Mostafavi S, Regev A, Rhoades A, Moodley D, Yoshida H, Mathis D, Benoist C, Nabekura T, Lam

V, Lanier LL, Brown B, Merad M, Cremasco V, Turley S, Monach P, Dustin ML, Li Y, Shinton SA, Hardy RR, Shay T, Qi Y, Sylvia K, Kang J, Fairfax K, Randolph GJ, Robinette ML, Fuchs A, Colonna M, Barrett NA, Austen KF. Expression profiling of constitutive mast cells reveals a unique identity within the immune system. Nat Immunol 2016;17:1–12. [PubMed: 26681455]

10. Amin K The role of mast cells in allergic inflammation. Respir Med 2012;106:9–14. [PubMed: 22112783]
11. Christo SN, Diener KR, Bachhuka A, Vasilev K, Hayball JD. Innate immunity and biomaterials at the nexus: Friends or foes. Biomed Res Int 2015;2015:1–23.
12. Marichal T, Tsai M, Galli SJ. Mast cells: Potential positive and negative roles in tumor biology. Cancer Immunol Res 2013;1:269–279. [PubMed: 24777963]
13. Norrby K Mast cells and angiogenesis. APMIS 2002;110:355–371. [PubMed: 12076253]
14. Beghdadi W, Madjene LC, Benhamou M, Charles N, Gautier G, Launay P, Blank U. Mast cells as cellular sensors in inflammation and immunity. Front Immunol 2011;2:37. [PubMed: 22566827]
15. Hiromatsu Y, Toda S. Mast cells and angiogenesis. Microsc Res Tech 2003;60:64–69. [PubMed: 12500262]
16. Wulff BC, Wilgus TA. Mast cell activity in the healing wound: More than meets the eye? Exp Dermatol 2013;22:507–510. [PubMed: 23802591]
17. da Silva EZM, Jamur MC, Oliver C. Mast cell function. J Histochem Cytochem 2014;62:698–738. [PubMed: 25062998]
18. Thevenot PT, Baker DW, Weng H, Sun M-W, Tang L. The pivotal role of fibrocytes and mast cells in mediating fibrotic reactions to biomaterials. Biomaterials 2011;32:8394–8403. [PubMed: 21864899]
19. Galli SJ, Borregaard N, Wynn TA. Phenotypic and functional plasticity of cells of innate immunity: Macrophages, mast cells and neutrophils. Nat Immunol 2011;12:1035–1044. [PubMed: 22012443]
20. Chillo O, Kleinert EC, Lautz T, Lasch M, Pagel J-I, Heun Y, Troidl K, Fischer S, Caballero-Martinez A, Mauer A, Kurz ARM, Assmann G, Rehberg M, Kanse SM, Nieswandt B, Walzog B, Reichel CA, Mannell H, Preissner KT, Deindl E. Perivascular mast cells govern shear stress-induced Arteriogenesis by orchestrating leukocyte function. Cell Rep 2016;16:2197–2207. [PubMed: 27524614]
21. Kolawole EM, McLeod JJA, Ndaw V, Abebayehu D, Barnstein BO, Faber T, Spence AJ, Taruselli M, Paranjape A, Haque TT, Qayum AA, Kazmi QA, Wijesinghe DS, Sturgill JL, Chalfant CE, Straus DB, Oskeritzian CA, Ryan JJ. Fluvastatin suppresses mast cell and basophil IgE responses: Genotype-dependent effects. J Immunol 2016;196:1461–1470. [PubMed: 26773154]
22. Douaiher J, Succar J, Lancerotto L, Gurish MF, Orgill DP, Hamilton MJ, Krilis SA, Stevens RL. Development of mast cells and importance of their tryptase and chymase serine proteases in inflammation and wound healing. Adv Immunol 2014;122: 211–252. [PubMed: 24507159]
23. Veiseh O, Doloff JC, Ma M, Vegas AJ, Tam HH, Bader AR, Li J, Langan E, Wyckoff J, Loo WS, Jhunjhunwala S, Chiu A, Siebert S, Tang K, Hollister-Lock J, Aresta-Dasilva S, Bochenek M, Mendoza- Elias J, Wang Y, Qi M, Lavin DM, Chen M, Dholakia N, Thakrar R, Ladk I, Weir GC, Oberholzer J, Greiner DL, Langer R, Anderson DG. Size- and shape-dependent foreign body immune response to materials implanted in rodents and non-human primates. Nat Mater 2015;14:643–651. [PubMed: 25985456]
24. Brown BN, Ratner BD, Goodman SB, Amar S, Badylak SF. Macrophage polarization: An opportunity for improved outcomes in biomaterials and regenerative medicine. Biomaterials 2012;33:3792–3802. [PubMed: 22386919]
25. Brown BN, Sicari BM, Badylak SF. Rethinking regenerative medicine: A macrophage-centered approach. Front Immunol 2014;5:349–311. [PubMed: 25101089]
26. Saino E, Focarete ML, Gualandi C, Emanuele E, Cornaglia AI, Imbriani M, Visai L. Effect of electrospun fiber diameter and alignment on macrophage activation and secretion of Proinflammatory cytokines and chemokines. Biomacromolecules 2011;12: 1900–1911. [PubMed: 21417396]
27. Garg K, Pullen NA, Oskeritzian CA, Ryan JJ, Bowlin GL. Macrophage functional polarization (M1/M2) in response to varying fiber and pore dimensions of electrospun scaffolds. Biomaterials 2013; 34:4439–4451. [PubMed: 23515178]

28. Keselowsky BG, Bridges AW, Burns KL, Tate CC, Babensee JE, LaPlaca MC, García AJ. Role of plasma fibronectin in the foreign body response to biomaterials. Biomaterials 2007;28:3626–3631. [PubMed: 17521718]
29. Garg K, Ryan JJ, Bowlin GL. Modulation of mast cell adhesion, proliferation, and cytokine secretion on electrospun bioresorbable vascular grafts. J Biomed Mater Res 2011;97A:405–413.
30. McClure MJ, Wolfe PS, Simpson DG, Sell SA, Bowlin GL. The use of air-flow impedance to control fiber deposition patterns during electrospinning. Biomaterials 2012;33:771–779. [PubMed: 22054536]
31. Walraven M, Hinz B. Therapeutic approaches to control tissue repair and fibrosis: Extracellular matrix as a game changer. Matrix Biol 2018;71–72:205–224.
32. Mosher DF. Plasma Fibronectin concentration: A risk factor for arterial thrombosis? Arterioscler Thromb Vasc Biol 2006;26:1193–1195. [PubMed: 16709950]
33. Enoksson M, Lyberg K, Moller-Westerberg C, Fallon PG, Nilsson G, Lunderius-Andersson C. Mast cells as sensors of cell injury through IL-33 recognition. J Immunol 2011;186:2523–2528. [PubMed: 21239713]
34. Lunderius-Andersson C, Enoksson M, Nilsson G. Mast cells respond to cell injury through the recognition of IL-33. Front Immunol 2012;3:82. [PubMed: 22566963]
35. Hu R, Zhang Y, Yang X, Yan J, Sun Y, Chen Z, Jiang H. Isoflurane attenuates LPS-induced acute lung injury by targeting miR-155-HIF1-alpha. Front Biosci (Landmark Ed) 2015;20:139–156. [PubMed: 25553444]
36. Lin F, Ren X-D, Pan Z, Macri L, Zong W-X, Tonnesen MG, Rafailovich M, Bar-Sagi D, Clark RAF. Fibronectin growth factor-binding domains are required for fibroblast survival. J Investigat Dermatol 2011;131:84–98.
37. Madurantakam PA, Cost CP, Simpson DG, Bowlin GL. Science of nanofibrous scaffold fabrication: Strategies for next generation tissue-engineering scaffolds. Nanomedicine 2009;4:193–206. [PubMed: 19193185]
38. Rnjak-Kovacina J, Wise SG, Li Z, Maitz PKM, Young CJ, Wang Y, Weiss AS. Tailoring the porosity and pore size of electrospun synthetic human elastin scaffolds for dermal tissue engineering. Biomaterials 2011;32:6729–6736. [PubMed: 21683438]
39. Rnjak-Kovacina J, Weiss AS. Increasing the pore size of electrospun scaffolds. Tissue Eng Part B Rev 2011;17:365–372. [PubMed: 21815802]
40. Veiseh O, Doloff JC, Ma M, Vegas AJ, Tam HH, Bader AR, Li J, Langan E, Wyckoff J, Loo WS, Jhunjhunwala S, Chiu A, Siebert S, Tang K, Hollister-Lock J, Aresta-Dasilva S, Bochenek M, Mendoza-Elias J, Wang Y, Qi M, Lavin DM, Chen M, Dholakia N, Thakrar R, Lacik I, Weir GC, Oberholzer J, Greiner DL, Langer R, Anderson DG. Size- and shape-dependent foreign body immune response to materials implanted in rodents and non-human primates. Nat Mater 2015;14:643–651. [PubMed: 25985456]
41. Pennel T, Zilla P, Bezuidenhout D. Differentiating transmural from transanastomotic prosthetic graft endothelialization through an isolation loop-graft model. J Vasc Surg 2013;58:1053–1061. [PubMed: 23541549]
42. Farrugia BL, Brown TD, Upton Z, Hutmacher DW, Dalton PD, Dargaville TR. Dermal fibroblast infiltration of poly(ε-caprolactone) scaffolds fabricated by melt electrospinning in a direct writing mode. Biofabrication 2013;5:1–25.
43. Soliman S, Sant S, Nichol JW, Khabiry M, Traversa E, Khademhosseini A. Controlling the porosity of fibrous scaffolds by modulating the fiber diameter and packing density. J Biomed Mater Res 2011;96A:566–574.
44. Ishizuka T, Okajima F, Ishiwara M, Iizuka K, Ichimonji I, Kawata T, Tsukagoshi H, Dobashi K, Nakazawa T, Mori M. Sensitized mast cells migrate toward the Agen: A response regulated by p38 mitogen-activated protein kinase and rho-associated coiled-coil-forming protein kinase. J Immunol 2001;167:2298–2304. [PubMed: 11490018]

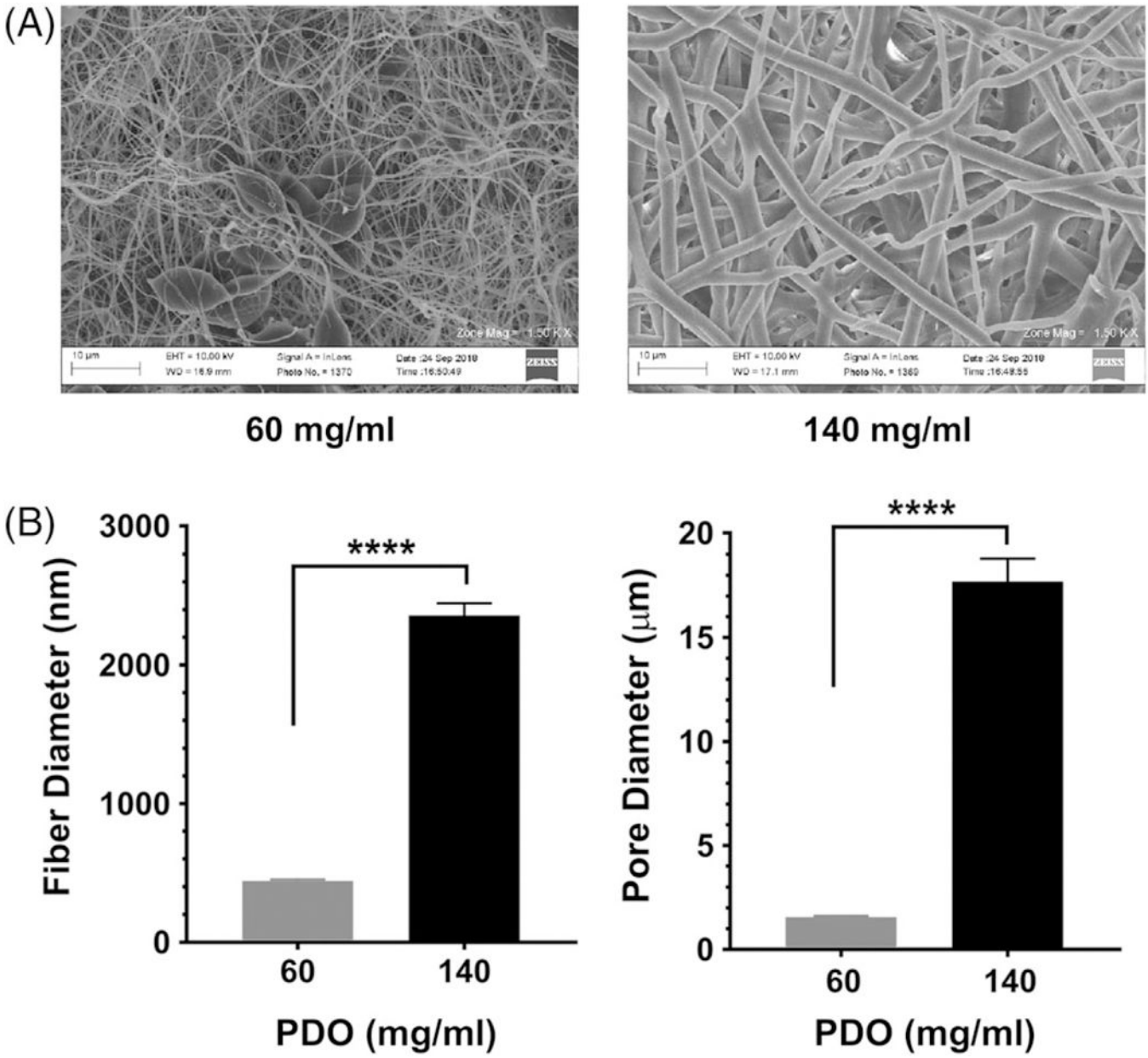

FIGURE 1.

Electrospun scaffold structure varies with PDO concentration. (A) Polydioxanone scaffolds of different polymer concentrations were electrospun, yielding scaffolds of different morphologies, as confirmed by SEM. (B) Electron micrographs were used to measure fiber and pore diameters of the scaffolds, calculated with ImageJ. Data shown are mean ± SEM from 25 to 60 measurements. ****, $p < 0.0001$.

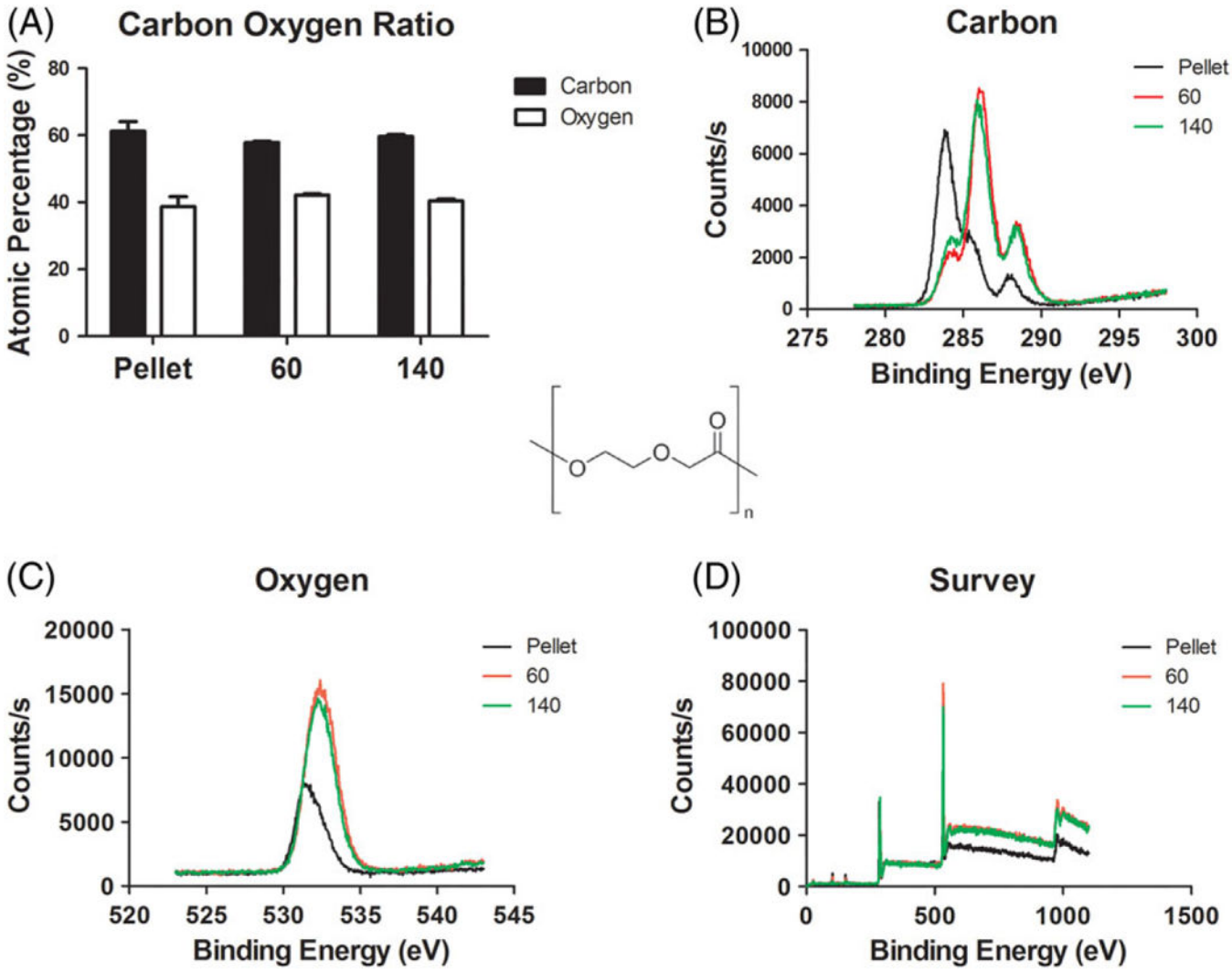

FIGURE 2.

Surface chemistry is unaffected by electrospinning and PDO concentration. (A) Carbon and oxygen ratios were similar between polydioxanone scaffold types and matched pure PDO pellets, positive control. (B) Carbon binding energy showed no differences in peaks when polydioxanone concentration was varied. Carbon binding energy for controls were lower, but not significant. (C) Oxygen binding energy showed no change. (D) Survey represents all binding energies and counts per second.

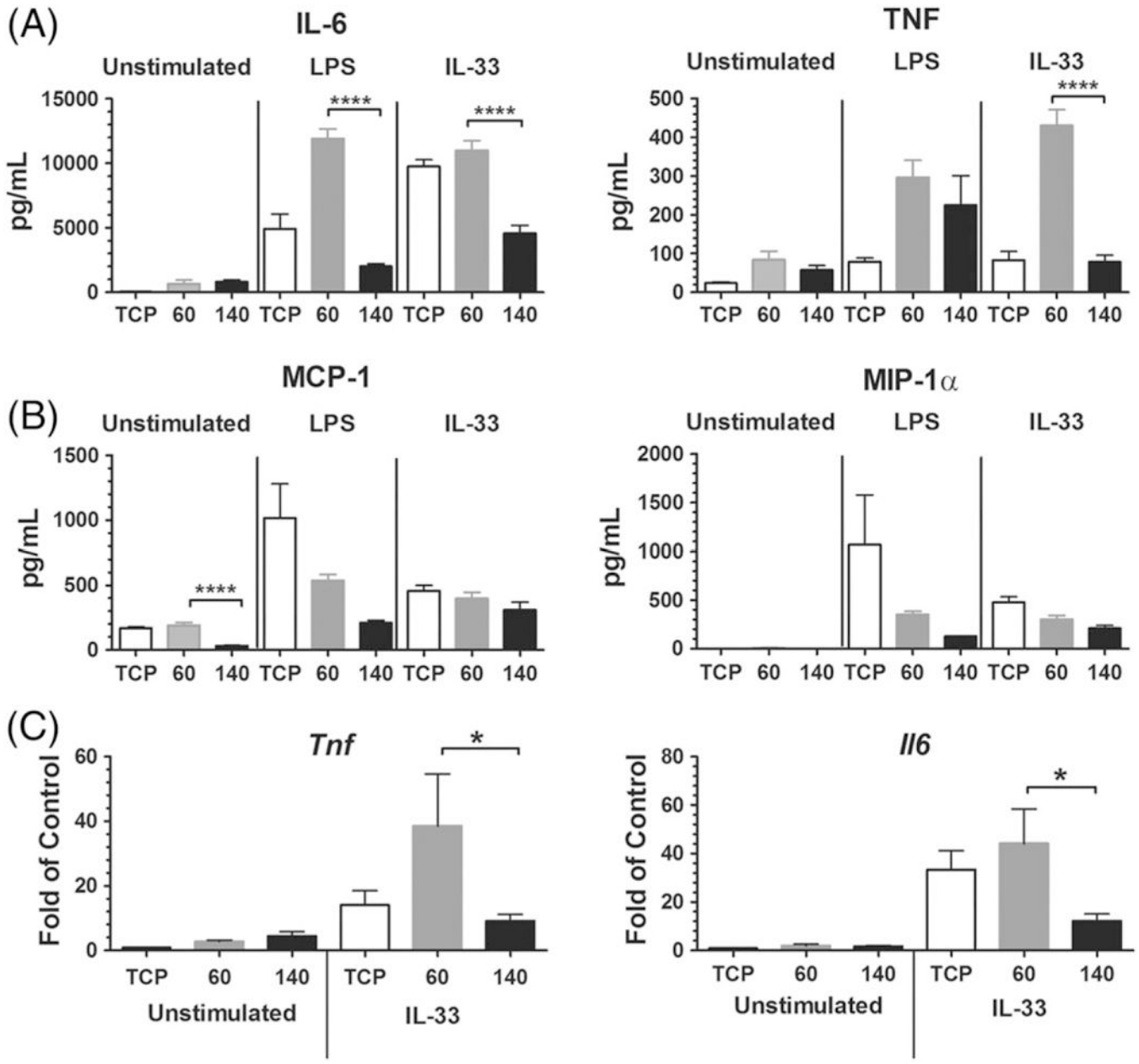

FIGURE 3.

Mast cell IL-6 and TNF production is altered on scaffolds of different morphologies. (A, B) BMMC were seeded on fibronectin-coated electrospun scaffolds for 48 h, then activated with LPS (1 μg/mL) or IL-33 (100 ng/mL). Supernatants were collected 16 h later and analyzed via ELISA for (A) IL-6 and TNF or (B) MCP-1 and MIP-1α. Results are mean ± SEM of 6–15 samples from two to three independent experiments. (C) BMMC were seeded and activated as in (A). RNA was harvested 3 h after activation and analyzed by RT-qPCR to detect mRNA for IL-6 and TNF. Results are mean ± SEM of 8–12 samples from two independent experiments.*, $p < 0.05$; ****, $p < 0.0001$.

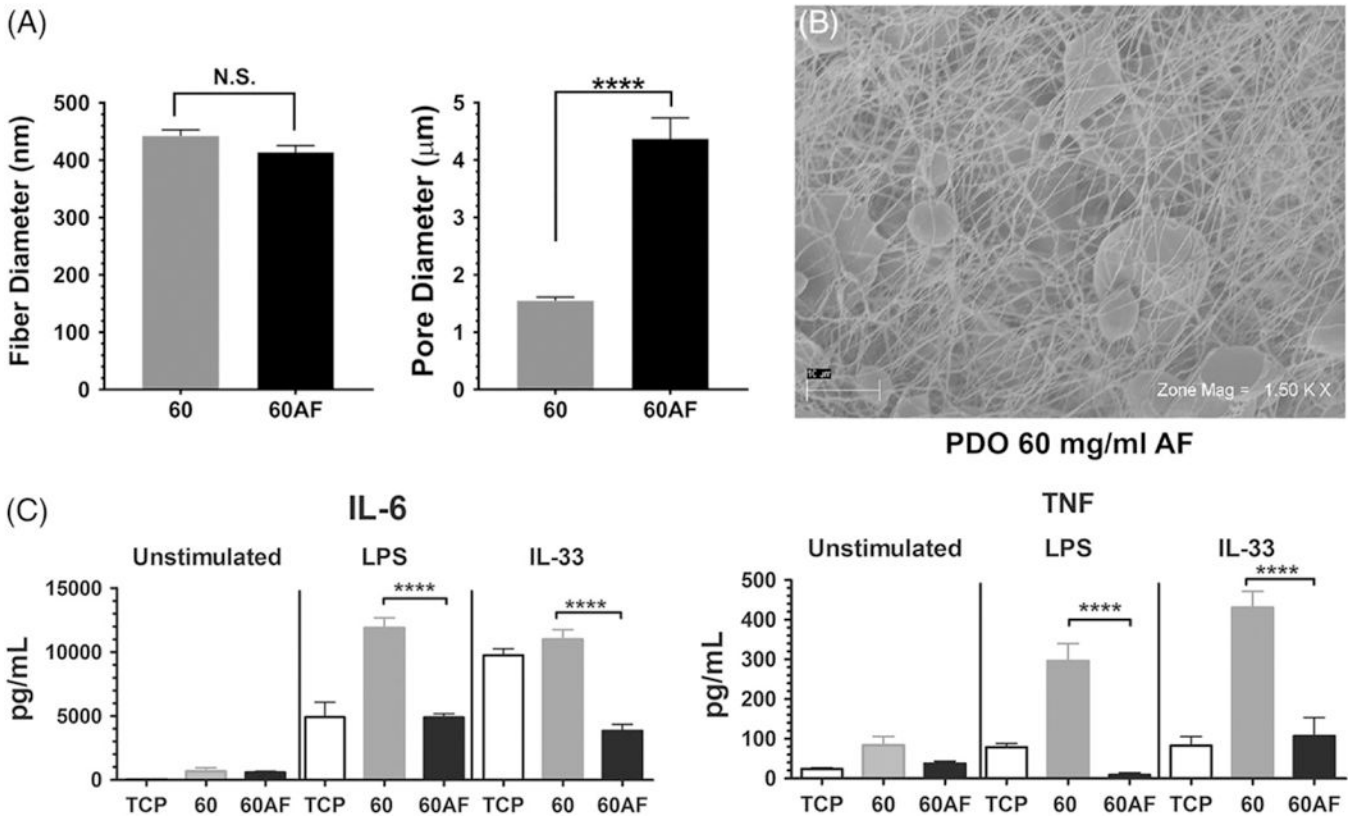

FIGURE 4.

I ncreasing pore size of 60 mg/mL electrospun scaffolds suppresses IL-6 and TNF production. (A) Fiber and pore diameters of the indicated scaffolds were calculated from SEM images shown at right. Data shown are mean ± SEM of 60 measurements. (B) Representative electromicrographs of a 60AF scaffold at two magnifications, showing regions of increased porosity. (C) BMMC were seeded on fibronectin-coated 60 and 60 AF electrospun scaffolds for 48 h and then activated with LPS (1 μg/mL) or IL-33 (100 ng/mL). Supernatants were collected 16 h later and analyzed via ELISA for IL-6 and TNF. Results are presented as mean ± SEM of nine samples from three independent experiments. ****, $p < 0.0001$.

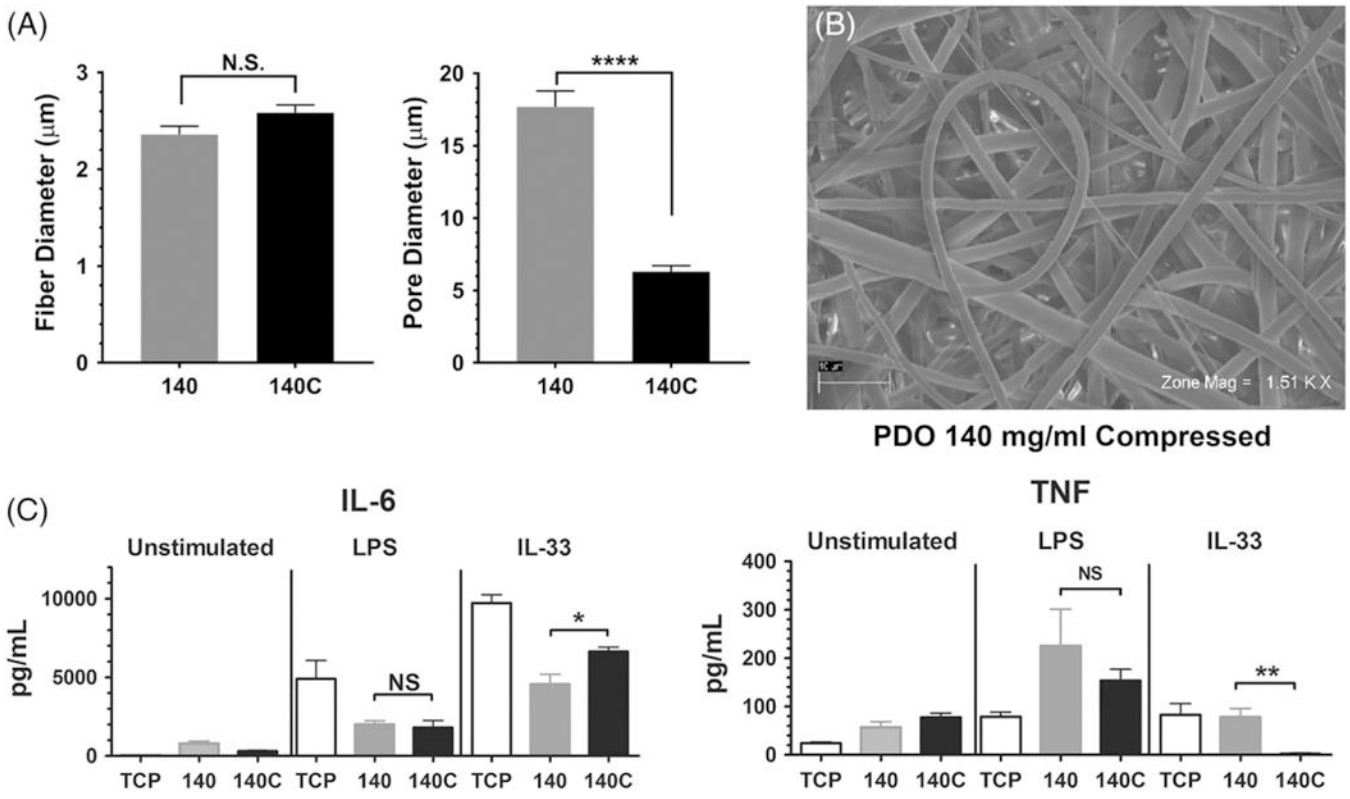

FIGURE 5.

Decreasing pore size of 140 mg/mL electrospun scaffolds has little effect on IL-6 and TNF production. (A) Fiber and pore diameters of the indicated scaffolds were calculated from SEM images. Fiber diameter was calculated from 25 to 40 measures; pore diameter is from 60 measurements. (B) Representative electromicrograph of a 140C scaffold. (C) BMMC were seeded on fibronectin-coated 140 and 140C electrospun scaffolds for 48 h and then activated with LPS (1 μg/mL) or IL-33 (100 ng/mL). Supernatants were collected 16 h later and analyzed via ELISA for IL-6 and TNF. Results are presented as mean ± SEM of nine samples from three independent experiments. *, $p < 0.05$; **, $p < 0.01$; ****, $p < 0.0001$; NS, not significant.

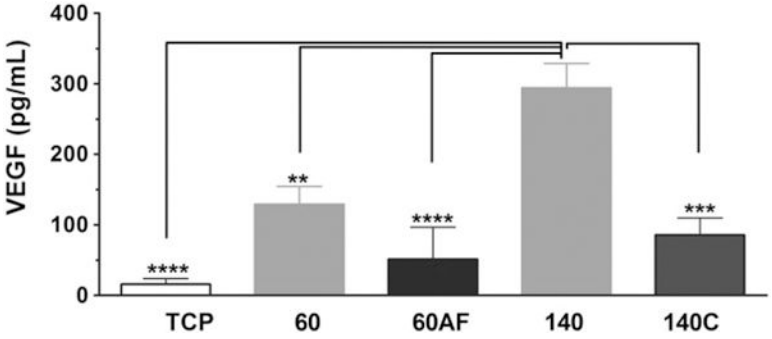

FIGURE 6.

VEGF production is altered by scaffold geometry. BMMC were seeded on the indicated fibronectin-coated electrospun scaffolds for 48 h and then activated with IL-33 (100 ng/mL). Supernatants were collected 16 h later and analyzed via ELISA for VEGF. Results are presented as mean ± SEM of eight to nine samples from three independent experiments. **, $p < 0.01$; ***, $p < 0.001$.